Characterization of a High Spatial Resolution γ Camera for Scanning HPGe Segmented Detectors

A. Hernández-Prieto, *Student Member, IEEE*, and B. Quintana

***Abstract*—Characterization of the electrical response of HPGe segmented detectors as a function of the interaction position is one of the current goals for the Nuclear Physics community in order to perform γ-ray tracking or even imaging with these detectors. For this purpose, scanning devices must be developed to achieve the signal-position association with the highest precision. With this aim, SALSA, a γ-camera-based scanning system, is under development at our laboratory. In this work, the optimization study aimed to obtain the best spatial resolution in the position-sensitive detectors employed as γ camera is described.**

***Index Terms*—LYSO crystal, position sensitive detector (PSD).**

I. Introduction

THE nuclear experiments to be performed in the new Radioactive-Ion Beam (RIB) facilities require the development of more efficient and sensitive γ-spectroscopy devices. With this objective, coaxial HPGe detectors with highly segmented electrical contacts, which are responsible for collecting the charge carriers released in each photon interaction, are used. Some relevant examples of these detectors can be found in international collaborations such as AGATA [1] or GRETA [2]. Contact segmentation enables us to determine the interaction points of a γ ray inside the Ge crystal, thus providing the data needed to reconstruct the γ-ray track. However, as an intermediate step, it is necessary to characterize the electrical response of the Ge crystal with respect to the position of the interaction point. At the same time, in order to explore in depth the Ge segmented detector capabilities, we have to reach the maximum precision in its characterization. To carry out this task, scanning systems are used. These are based on the measurement of a radioactive source with ancillary detectors devoted to detecting in coincidence those photons which generate a signal in the Ge detector to be characterized. Most scanning systems use the mechanical movement of a collimated source with respect to the detector to determine the γ-ray interaction position in the Ge crystal [3]. Their main drawbacks are the long time needed to scan the whole detector, the high activity required in the source and the precision limited by the mechanics. However, a virtual collimation [4] becomes an alternative by employing the two co-linear 511-keV photons emitted in the annihilation of the positron [5]. Then, the photon direction must be determined with a Position Sensitive Detector (PSD).

A PSD can be built, for instance, with a scintillator crystal coupled to a Position Sensitive PhotoMultiplier Tube (PSPMT). With such a device, the interaction position of the photon at the scintillator can be determined by using the appropriate algorithm. This type of PSD was originally developed by H. O. Anger [6], whose work is considered as the starting point of modern γ cameras. Concerning his approach, a new milestone was reached with the commercial introduction of small PSPMTs, which enabled the development of very compact miniature gamma cameras [7]. However, other options based on gas-filled detectors have also been studied and proposed for a wide range of applications [8], [9], [10].

Since the original work of H. O. Anger, the readout techniques and the associated image reconstruction algorithms used with scintillators have evolved significantly. A new multi-anode readout method, together with a suitable image reconstruction algorithm, was investigated by Bird *et al.* [11] by using a multi-channel very-large-scale integration (VLSI) charge-sensitive amplifier array. In the same year, Truman *et al.* [12] applied the position-sensitive PMT readout as well as the peak-fitting algorithm, both proposed by Bird *et al.* to pixellated CsI(Tl) arrays, obtaining improved resolutions. Recently, this readout method has been applied to a scanning system based on a virtual collimation, such as the one presented in this paper [13]. Finally, the arrival of the flat-panel-type multianode photomultiplier tube [14] afforded large detection areas, allowing new image reconstruction algorithms to be explored by applying neural networks [15] or simply by narrowing the PSPMT signal readout [16].

In the scanning system proposed here, the PSDs are made of continuous lutetium yttrium oxyorthosilicate (LYSO) scintillating crystal [17] and flat-panel PSPMTs, which provide full acquisition of the light distribution produced by the interacting γ rays in the scintillator crystal. Our objective is to improve the accuracy of the interaction position obtained with a large detection area γ camera. With this aim, the algorithms employed to obtain this position are investigated.

Currently, the most common algorithms to determine the γ-ray interaction position in commercial γ cameras are based on the original Anger's Logic [6] or its later improvement [16]. When applied to PSDs using PSPMTs with 64 pixels, such as the ones used in this work, this method enables a reduction in the PSPMT outputs, usually from 64 to 4 outputs per PSPMT.

Manuscript received July 10, 2012; revised January 14, 2013; accepted October 16, 2013. Date of publication November 20, 2013; date of current version December 11, 2013. This work was supported in part by Grants FPA2008-06419 and FPA2008-03774, in part by Consolider CSD2007-00042 by MICINN Spain, and in part by GR12 from the Junta de Castilla y León.

The authors are with the Laboratorio de Radiaciones Ionizantes, University of Salamanca, 37007 Spain (e-mail: alvaro.prieto@usal.es).

Color versions of one or more of the figures in this paper are available online at http://ieeexplore.ieee.org.

Digital Object Identifier 10.1109/TNS.2013.2287252

This requires special hardware in the readout stage, consisting of a matrix of resistances. The reduction in the number of outputs is possible because the Anger's Logic works with the signal projections on the X- and Y-axes. However, when 64 outputs are available, calculation of the interaction position using the X- and Y-projections leads to a loss of information regarding the light distribution, which is particularly critical at the edge of the crystal. This effect, associated with the use of Anger's Logic, spoils the resolution of our system, which is actually based on four coupled PSDs.

In this work, we aim to improve the behaviour and the resolution of the four optically coupled PSDs employed in SALSA, which work together. This objective requires a study to optimize both the PSPMT readout electronics and the position location algorithm. Regarding the latter, we propose in Section III the application of a Gaussian peak-fitting algorithm to the full experimental light distribution of LYSO crystals based on Least Squares. A similar solution was previously explored by Bird *et al.* [11] and Truman *et al.* [12] but using CsI(Tl) and NaI(Tl) scintillator crystals. Before Section III, our scanning system, together with the details of its γ camera and associated readout electronics, are presented in Section II. Section IV describes the experimental measurements carried out with the scope to characterize the PSDs. In Section V, we examine the results obtained regarding the light distribution response all over the PSD surface. The better we reproduce the light distribution numerically, the lower the uncertainty in the position determination and, therefore, the better the PSD capability to discern different γ-ray interaction points. We also apply these results to evaluate the linearity of the PSD that enables us to offer the obtained resolutions in terms of geometrical distances into the LYSO crystals. In Section VI, some conclusions are given.

II. Description of the γ Camera

The operation of the SAlamanaca Lyso-based Scanning Array (SALSA) is based on the determination of the spatially correlated directions of the two photons following a $\beta^+\beta$ annihilation. For this purpose, a PSD is needed to detect one of the two photons and to disentangle its interaction position in the PSD, bearing in mind that the lower the position uncertainty, the higher the resolution of the scanner. There is also a contribution to the position determination uncertainty in the PSD which comes from the finite size of the ^{22}Na source and from the non-collinearity of the two generated 511 keV photons. These two effects are negligible in our system given the short distances between the elements of SALSA and the point-like ^{22}Na source with only 0.25 mm diameter [18]. Accordingly, a ^{22}Na source that provides two simultaneous 511-keV γ rays in opposite directions and a large detection area PSD with scintillators capable of determining the directions of the 511-keV photons form part of SALSA. The γ camera developed to achieve high performance consists of four high-spatial-resolution sets, each one made up of continuous LYSO crystals, $52 \times 52 \times 5$ mm^3 in size. LYSO crystals have a high self activity, mainly from the β decay of the ^{176}Lu isotope, which represents 2.6% of natural Lu. The usual LYSO intrinsic backgrounds are around 260 counts s^{-1} cm^{-3}, as can be seen, together with the specific characteristics of LYSO crystals, in the work of Pidol *et al.* [17].

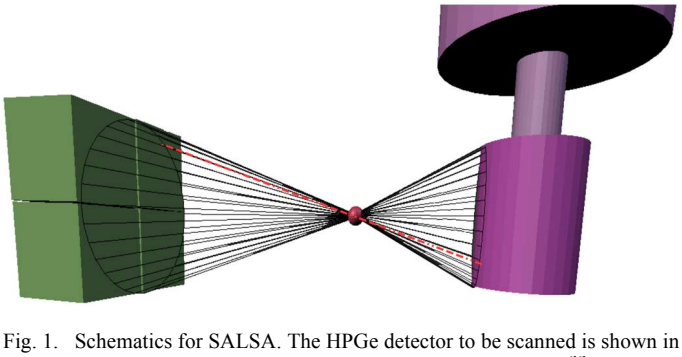

Fig. 1. Schematics for SALSA. The HPGe detector to be scanned is shown in purple, whereas the γ camera is depicted in green. The point-like ^{22}Na source is drawn red.

The choice of the crystal thickness was done by performing a Monte Carlo simulation, looking for a balance between high peak-to-total ratios at 511 keV and low probability of full photon-energy absorption by multiple interactions at 511 keV, which enhances the signal of interest against the ones due to multiple interactions that spoil the position resolution of the LYSO crystals. Thicknesses from 3 mm up to 10 mm were implemented in the MC simulations. A thickness of 5 mm is considered a good agreement, providing a peak-to-total ratio (P/T) at 511 keV of 16% and a peak efficiency at 511 keV of 12.8%, both calculated from the simulated total spectrum corresponding to a ^{22}Na source. The readout of the crystal is performed with a position-sensitive photomultiplier tube (PSPMT) model H10966A-100 by Hamamatsu. Each PSPMT has an output of 64 channels, one per pixel, plus an additional channel corresponding to the last dynode signal. In our configuration, all channels coming from each PSPMT are read. This affords 260 electronic signals, providing a 104×104 mm^2 total detection area. The optical coupling of the four LYSO-PSPMT sets is made in the same X-Y plane, as shown in Fig. 1. In SALSA, the ^{22}Na source is located between the PSDs and the HPGe detector, as also shown in Fig. 1.

In order to integrate and digitize the 260 electronic signals coming from the PSDs, they were AC-coupled into eight model V792 charge-to-digital conversion (QDC) VME modules from CAEN, having an input range from 0 to 400 pC and a digital resolution of 12 bits. The readout of the 260 QDC channels from the PSPMT anodes and dynodes is achieved via the MultiBranch System (MBS) [19]. This system runs under the Lynx-real-time operative system in a VME PowerPC platform RIO4-8072RE 1 GHz from CES [20]. The online and offline analyses are performed using the Object Oriented Online Offline system Go4 [21], based on the ROOT package of CERN [22]. Other modules are fast leading-edge discriminators (LED) model N840 from CAEN, timing-filter amplifiers TFA-474 from ORTEC and gate-and-delay generators model GG8020 also from ORTEC. The schematic of the electronics is shown in Fig. 2, where the logic process aimed at ensuring the coincidence between the PSDs and the scanned detector is also indicated.

Although the same high voltage is applied to all the anodes of a PSPMT, a different response is obtained in terms of signal amplification. This causes distortions in the image reconstruction algorithm. To solve this problem, the individual anode readout is

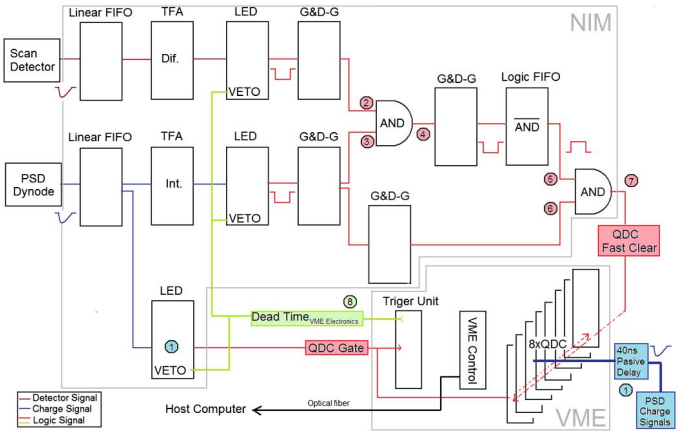

Fig. 2. Schematics for SALSA electronic set-up.

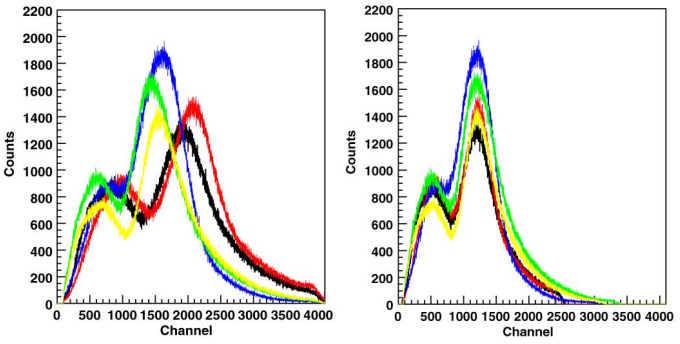

Fig. 3. On the left, the raw QDC pulse height spectra for five representative anodes. On the right, the pulse height spectra after calibration.

used in order to correct the gain deviation between anodes. The required adjustment will ensure a homogeneous response along the whole γ camera surface, as can be seen in Fig. 3, where only 4 channels are shown in order for the graphics to be more understandable.

To perform the anode gain matching, the γ camera was fully illuminated using the same 1-MBq ^{22}Na source as the one used in the scanning measurements. In this way, no additional source is needed to carry out the procedure. Measurements were performed with the source placed between the PSD and a NaI(Tl) detector, the PSD-to-source and source-to-NaI(Tl) distances being 72.4 mm and 75.0 mm, respectively. The purpose of the NaI(Tl) detector is to perform measurements with the system's coincidence electronics (Fig. 2), taking advantage of the optimization already performed for the scanning measurements. The fact that the γ-camera's data acquisition runs in coincidence with the NaI(Tl) detector also reduces background due to the LYSO self-activity peak at 508.66 keV. This peak is due to the true-coincidence summing of two in-cascade emissions from ^{176}Lu: the 201.83-keV and 306.82-keV ones. As far as the scanning procedure is concerned, these events are measured by the γ camera in the same energy window as the 511-keV ones, spoiling the reliability of the characterization. Count rates at 508.66-keV of 0.87 counts s^{-1} are obtained in the γ camera with the coincidence electronics against a count rate of 66 counts s^{-1} without coincidences. Presumably, the use of coincidences brings some disadvantages to the anode gain matching procedure because of the reduction of the 1274.57-keV peak area. However, this peak is not even observed in the anode spectra without coincidences, which let us match the anode gains just with the 511-keV peak. The count rate at 1274.57 keV recorded at the dynode without coincidences is 0.11 counts s^{-1}, which gives rise to a number of counts in the anodes lower than the detection limit at this energy. The count rate at 1274.57 keV in the γ camera dynode spectrum measured in coincidence is 0.05 counts s^{-1}, which causes count rates in the anodes lower than the detection limit. The 1274.57-keV peak is seen just in the dynode in ideal conditions. A peak efficiency at 1274.57 keV of 1.1% is obtained against a value of 11.9% at 511 keV when the ^{22}Na source is collimated and its emissions impinge in a central anode of the PSD. Therefore, only the 511-keV peak was used to determine the gain factor corresponding to each anode. Taking into account that the 511-keV peak is the one used in the image reconstruction, this did not represent a severe setback. Gain factors were obtained relative to a reference value, given by one of the anodes. After the anode gain matching has been accomplished, the γ camera is ready to operate. The right part of Fig. 3 shows the calibrated spectra.

III. Position Location Algorithm

SALSA takes advantage of both the continuous scintillator crystals of the γ camera and the complete readout of all the signals coming from the scintillators. By exploring the two-dimensional (2D) shape of light distribution in the PSDs, the later determination of the position interaction event by event can be achieved by performing a fit to a parametric shape function with an optimized number of parameters. To reduce the number of fitting parameters, a previous characterization of the light distribution is done. To characterize the light distribution of our γ camera, an algorithm was developed, which proceeds as follows:

- In a first stage, a background fit and its further subtraction from the experimental data is performed in order to remove possible effects due to both the light reflectivity on the edges of the scintillator crystal and the electronic noise.
- In a second stage, a fit of a parametric Gaussian function to the net experimental distribution is carried out. The selection of the Gaussian function is purely empirical, based on the observation of the experimental light distribution provided by each of the pixels. Then, a statistical test is applied to check if the model and experimental data differ. The fitting was accomplished using ROOT's implementation of the TMinuit minimization algorithm [23].

The Gaussian function used to shape the light distribution is as follows:

$$f(x,y) = Ae^{-\frac{1}{2}\left(\frac{(x-x_0)^2}{\sigma_x^2}+\frac{(y-y_0)^2}{\sigma_y^2}\right)}. \quad (1)$$

This function has five parameters: A, x_0, σ_x, y_0 and σ_y. These parameters correspond, respectively, to the maximum amplitude of the light distribution, the x coordinate of the centroid position, the light distribution width in the x direction, the y coordinate of the centroid position and the light distribution width along the y direction. With the Gaussian function given in (1),

the light distribution is assumed to have X- and Y- axes as symmetry axes, both being parallel to the crystal edges and each one orthogonal with respect to the other. By using this Gaussian function, it is possible to obtain not only the centroid of the Gaussian, (x_0, y_0) and, as a consequence, the interaction position in the γ-camera plane, but also the light distribution width (σ_x, σ_y).

The output of the fit consists of the parameter values together with their uncertainties. The uncertainties are obtained from the parameter covariance matrix, $\{c(a_i, a_j), i, j = 1, \ldots, n\}$, where a_i and a_j are, respectively, the ith and jth fitting parameter and n is the total number of parameters. The covariance matrix's diagonal terms corresponding to the parameters x_0 and y_0 provide the uncertainty in the γ-ray interaction position in the γ camera. This uncertainty, together with the uncertainty in the β^+ annihilation position within the ^{22}Na source, determines the total uncertainty of the position inside the HPGe segmented detector.

Since the method described in this work allows us to obtain not only shape but also light distribution width, it is possible to study, after a set of events for different positions, whether width remains constant over all the γ-camera surface or not. If so, the σ_x and σ_y values can be fixed, reducing the number of parameters in the light distribution fit of an individual event. Position determination is done event by event when the characterization system scans a HPGe detector; therefore, such a reduction contributes to decreasing uncertainty in the position parameters.

IV. Experimental Method

The ^{22}Na source was placed in different collimated positions in order to acquire the set of measurements needed to characterize the light distribution response in the γ camera. For this task, a 1-mm-hole and 50-mm-length lead collimator coupled to a high precision X-Y support, which allows the entire surface of each PSD to be covered, was used. The distance between the face of the collimator and the PSD was 12 mm, affording a 1.48-mm spot due to the divergence of the beam. The collimated position pattern employed in the measurements of each individual PSD is shown in Fig. 4. Pixels are identified by the row and column labels shown in this figure. Note that at this stage each PSD has been characterized independently. In order to clarify the results presented in this work, the serial number of the PSDs: ZK0021, ZK0084, ZK0065 and ZK0079, are used to identify each of them independently.

Measurements in each collimator position were carried out by running the system in coincidence mode between the PSD and a NaI(Tl) detector. Once a set of 10^6 events have been accumulated, the normalized light distribution corresponding to each position was obtained, together with the associated standard deviation.

V. Results

A. Light-Distribution Characterization

The Gaussian function of Eq. (1) is fitted to the normalized light distributions obtained at each collimator position. Fig. 5 shows an illustrative Gaussian fit for a particular position in the centre of one the PSDs.

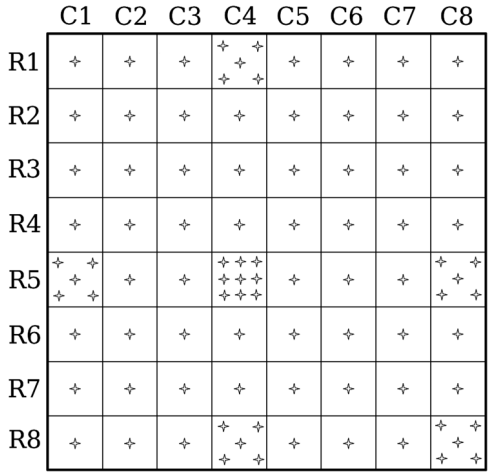

Fig. 4. Pattern of positions where a measurement was made with the collimated source.

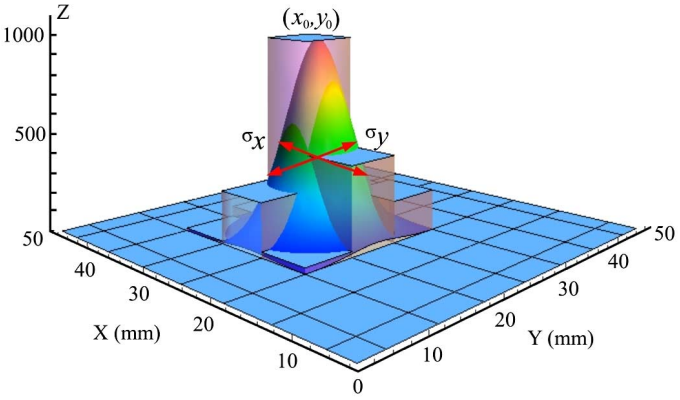

Fig. 5. Experimental light distribution represented by cuboids corresponding to a particular position on the X-Y plane of the ZK0021 PSD. The fitted distribution is also shown by a smooth Gaussian shape.

With all the fits done to the light distributions measured at different pixels, the assumption that the X- and Y-axes are the symmetry axes can be checked. In Table I, σ_x values are given for positions (pixels) with constant values of the Y-coordinate (see Fig. 4). In Table II, the σ_y values are shown corresponding to pixels with a constant X-coordinate (see also Fig. 4). The values given in Table I do not differ statistically. The same is the case of the values given in Table II. Therefore, σ_x and σ_y kept constant along the X- and Y-axes which shows that they can be taken as symmetry axes of the light distribution. If light distribution had other symmetry axes, the distribution width projected on X- and Y-axes should change gradually.

Given that the method proposed to obtain the interaction position relies on the light-distribution fit to a Gaussian function in which σ_x and σ_y are constant, it is necessary to select the best estimation of these widths. Therefore, a statistical study is required to decide what values to take. We constructed the experimental probability distribution of both σ_x and σ_y by taking their values from the the light-distribution fits corresponding to

TABLE I
VALUES FOR σ_x WHEN THE X-COORDINATE (22.0 ± 0.1 MM) REMAINS CONSTANT AND THE Y-COORDINATE VARIES

Pixel	Y-coordinate (mm)	σ_x (mm)
R8C4	4	3.71±0.11
R7C4	10	3.62±0.49
R6C4	16	3.25±0.86
R5C4	20	3.35±0.11
R4C4	28	3.55±0.91
R3C4	34	3.23±0.72
R2C4	40	3.85±0.99
R1C4	46	3.27±0.20
MEAN VALUE		3.45±0.73

TABLE II
VALUES FOR σ_y WHEN THE Y-COORDINATE (22.0 ± 0.1 MM) REMAINS CONSTANT AND THE X-COORDINATE VARIES

Pixel	X-coordinate (mm)	σ_y (mm)
R5C1	4	3.69±0.10
R5C2	10	3.02±0.81
R5C3	16	3.64±0.13
R5C4	20	3.47±0.06
R5C5	28	3.11±0.76
R5C6	34	3.09±0.86
R5C7	40	3.44±0.71
R5C8	46	3.66±0.38
MEAN VALUE		3.38±0.29

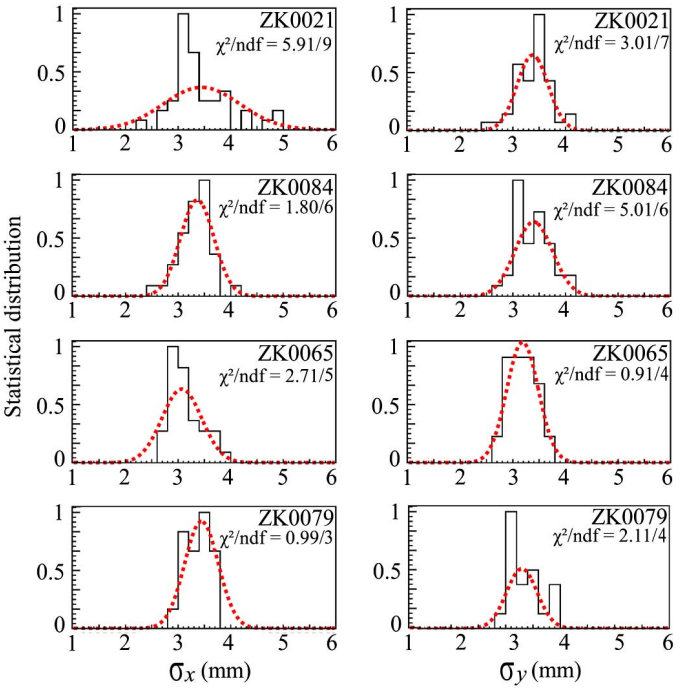

Fig. 6. Frequency diagrams corresponding to the light distribution width in each PSD for the different collimator positions. On the left, the σ_x component and, on the right, the σ_y component. χ^2/ndf represents the χ^2 statistic value per degrees of freedom.

all the collimated positions for each PSD. The values are represented in a histogram grouping all the σ values in 0.2-mm intervals. The number of bars depends on the data dispersion. To characterize this statistical distribution, we compared it, by a χ^2 test, with a Gaussian function because in this case the average

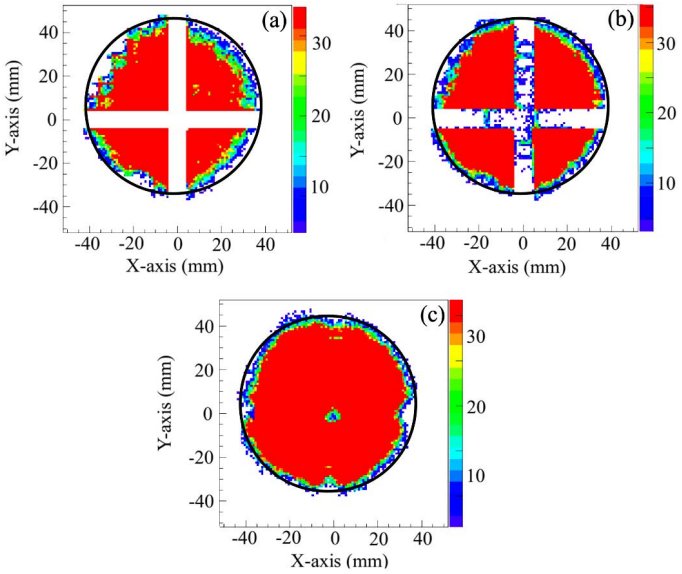

Fig. 7. Images of the coincidence NaI(Tl) detector using our four PSDs as γ camera obtained when the position interaction in the NaI(Tl) X-Y plane is calculated with (a) the Anger's Logic algorithm, (b) the Gaussian fit without fixing the light distribution width and (c) the Gaussian fit fixing the light distribution width. The real outline of the NaI(Tl) detector is drawn in black.

TABLE III
MEAN LIGHT-DISTRIBUTION WIDTHS FOR EACH PSD

γ−camera	σ_x (mm)	σ_y (mm)
ZK0021	3.45±0.73	3.38±0.29
ZK0084	3.36±0.32	3.39±0.36
ZK0065	3.07±0.37	3.18±0.30
ZK0079	3.44±0.32	3.30±0.28

value corresponds to the maximum likelihood value. Additionally, with this test we check the random nature of the fluctuation of the σ_x and σ_y widths. If the fluctuation was random, the distribution mean value would correspond to the most probable value. The results are shown in Fig. 6.

The mean values associated with the statistical distributions for each σ_x and σ_y component together with their uncertainties are given in Table III. These values will be fixed in order to reduce the number of free parameters in the light distribution Gaussian fit when performed event by event, i.e. with SALSA working in a real situation. This allows not only a reduction in the uncertainty of the centroid determination but also an increase in the the useful field of view in the PSD, which becomes a solution for the blind zones that appear in the junctions between each PSD.

Fig. 7 shows the images corresponding to the X-Y plane of the NaI(Tl) detector when it is fully illuminated with the ^{22}Na source and compares them with the real outline. These images were acquired with the four PSDs working together as a γ camera. In (a) the data acquired were treated with Anger's Logic algorithm. The blind zone is clearly visible between the PSDs due to the poor behaviour of the algorithm at the edge of the scintillator crystal. Blind zones start being filled and the field of view increases in (b), where the Gaussian fit of the light distribution is applied event by event without fixing the light distribution width with respect to (a). In (c) the blind zone is

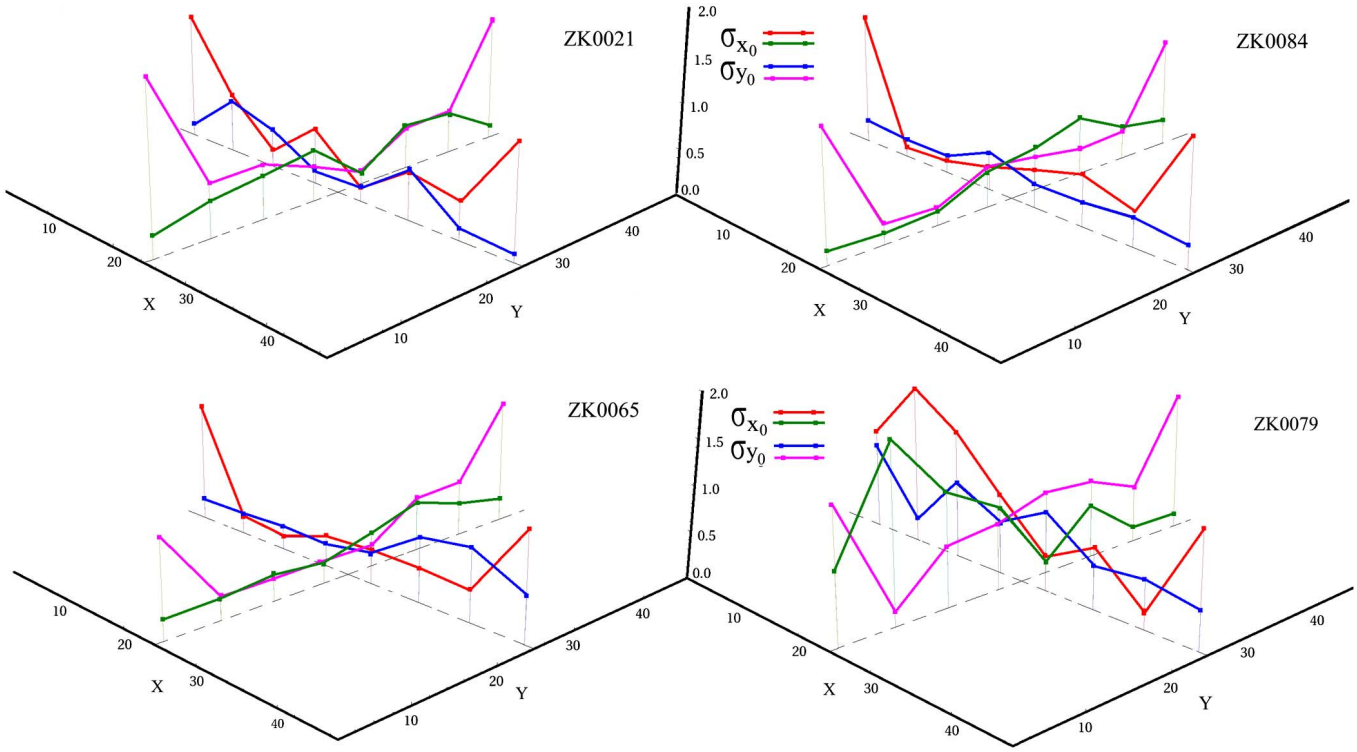

Fig. 8. Experimental uncertainties in the centroid determination σ_{x_0} (purple) and σ_{y_0} (blue) obtained for each PSD versus the collimated positions for a particular scanning direction in which the Y-coordinate is kept constant. The same uncertainties but for a scanning direction in which the X-coordinate is now kept constant are depicted in green for σ_{x_0} and brown for σ_{y_0}.

strongly suppressed when the light distribution width is fixed in the Gaussian fit with the values given in Table III, and the field of view is maximum.

B. Spatial Resolution

The uncertainty values for the centroid determination of the normalized light distribution, σ_{x_0} and σ_{y_0}, in the four PSD surfaces provide the spatial resolution of the γ camera. The ensemble of values obtained for the different collimated interaction positions on the X-Y plane of the γ-camera were studied.

As seen in Fig. 8, we observe that the uncertainty σ_{x_0} worsens when approaching the edge of the γ camera for a scanning direction in which the Y-coordinate of the collimated points is kept constant and the X-coordinate varies between the two edges of the crystal. However, σ_{y_0} remains almost constant. This situation can be understood graphically in Fig. 9(a) which shows that when approaching the X edge the experimental data set corresponds to a light distribution partially acquired for the X component. The same effect, but for a scanning direction in which the X-coordinate of the collimated points is kept constant and the Y-coordinate varies from one edge of the crystal to the other, is observed for σ_{y_0}. As shown in Fig. 8, the σ_{x_0} values remain almost constant while the σ_{y_0} ones worsen when reaching the edge of the Y-coordinate of the crystal. Fig. 9(b) shows how that light distribution is incompletely acquired for the Y component.

The mean values and, therefore, the spatial resolution of each PSD are shown in Table IV. The goodness-of-fit parameter remains constant at $\simeq$ 1 throughout the central regions of the PSDs, and rises consistently to $\simeq 1.5$ in the corner and edge regions. In Table V the σ_{x_0} and σ_{y_0} averaged values are presented separately for the central and edge zones in the PSDs. The uncertainties remain practically constant over the whole surface of the PSD except in the problematic edges, the X-axis for the σ_{x_0} component and the Y-axis for σ_{y_0} one, as shown in Fig. 8.

TABLE IV
MEAN VALUES FOR THE UNCERTAINTIES IN THE LIGHT DISTRIBUTION CENTROID DETERMINATION ALL OVER THE SURFACE OF EACH PSD

	X-axis		Y-axis	
$\gamma-$camera	σ_{x_0} (mm)	σ_{y_0} (mm)	σ_{x_0} (mm)	σ_{y_0} (mm)
ZK0021	0.65	0.36	0.28	0.73
ZK0084	0.59	0.33	0.27	0.56
ZK0065	0.54	0.32	0.42	0.58
ZK0079	0.95	0.74	0.61	0.87

C. Linearity

Linearity allows us to check what the final quality of our images will be, since we relate the real positions to the reconstructed ones through linearity. From the measurements acquired at the collimated positions, we tested the linearity of each PSD. In Fig. 10, mechanical positions are plotted versus the reconstructed ones, together with the line representing the ideal behaviour. One can see that the behaviour of our γ camera is practically ideal since the reconstructed positions are in very good agreement with the mechanical ones. The mean and maximum deviations for X- and Y-coordinates and for each PSD are listed in Table VI.

TABLE V
AVERAGED VALUES IN THE CENTRAL AND EDGE AREAS OBTAINED IN THE LIGHT DISTRIBUTION CENTROID DETERMINATION FOR EACH PSD

	X-axis (Centre)		X-axis (Edges)		Y-axis (Centre)		Y-axis (Edges)	
$\gamma-$camera	σ_{x_0} (mm)	σ_{y_0} (mm)	σ_{x_0} (mm)	σ_{y_0} (mm)	σ_{x_0} (mm)	σ_{y_0} (mm)	σ_{x_0} (mm)	σ_{y_0} (mm)
ZK0021	0.43	0.42	1.32	0.19	0.33	0.44	0.11	1.61
ZK0084	0.31	0.36	1.40	0.22	0.28	0.31	0.25	1.31
ZK0065	0.30	0.34	1.25	0.24	0.43	0.37	0.37	1.22
ZK0079	0.71	0.66	1.18	0.48	0.58	0.67	0.69	1.49

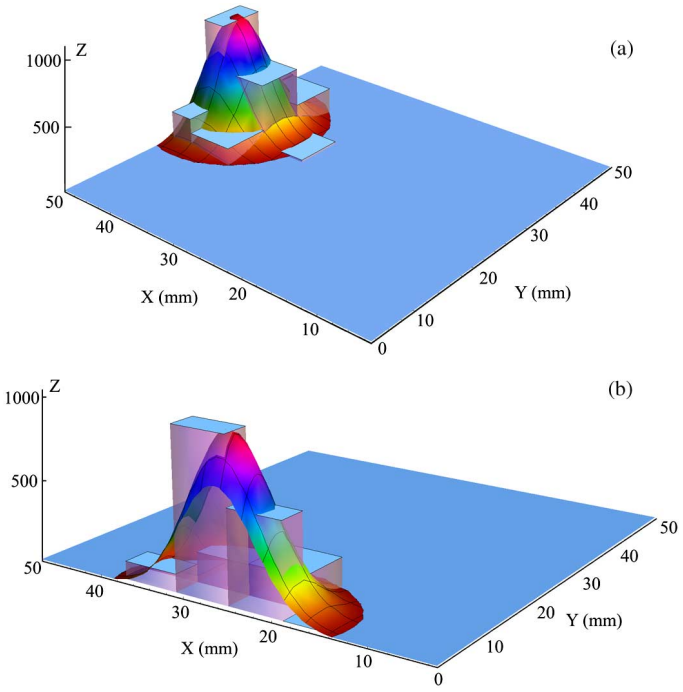

Fig. 9. Light distribution Gaussian fit with an incomplete set of experimental points when the interaction position is close to the edge of the PSD; (a) at the X-axis border and (b) at the Y-axis border.

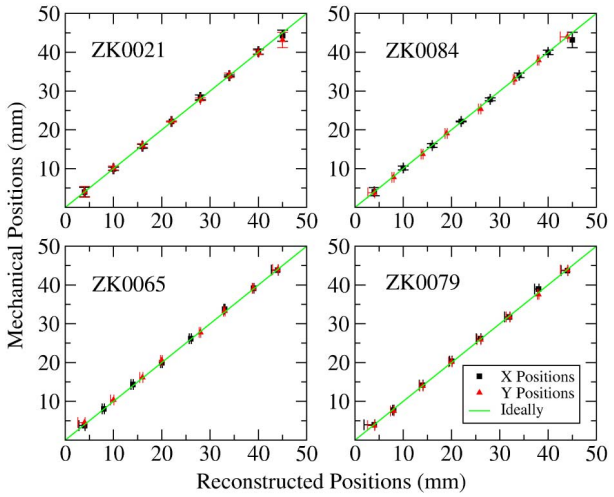

Fig. 10. X- and Y-coordinates of the mechanical positions versus X- and Y-coordinates of the reconstructed ones for the four PSDs. The green diagonal line illustrates the linearity performance of an ideal detector.

D. Point Spread Function

Another discussion concerning the spatial resolution of our detector is the Point Spread Function (PSF) [24], measured as the FWHM of the distribution of positions x and y. This quantity measures the ability of the system to distinguish between closely spaced centroids. In order to determine this value we used the collimated measurements described in Section IV. Fig. 11 shows an example of the distribution of positions x and y obtained from the Gaussian fit when we move the collimated source in 2-mm steps inside a single central pixel. The response to these movements can clearly be seen, both, along X- and Y-directions.

TABLE VI
MEAN AND MAXIMUM DEVIATION VALUES BETWEEN THE MECHANICAL AND RECONSTRUCTED POSITIONS FOR EACH PSD

	Mean deviation (mm)		Maximum deviation (mm)	
$\gamma-$camera	X-coord.	Y-coord.	X-coord.	Y-coord.
ZK0021	0.28	0.31	0.75	1.35
ZK0084	0.31	0.20	1.25	0.65
ZK0065	0.24	0.29	0.75	0.55
ZK0079	0.30	0.23	0.95	0.45

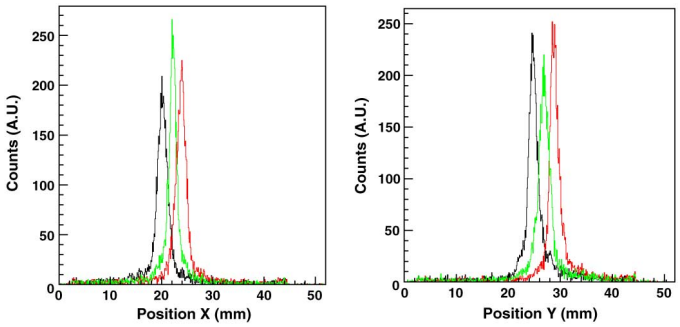

Fig. 11. On the left the distribution of positions x for the three positions inside the pixel. On the right the distribution of positions y for these three positions. A set of 10^6 events are used for each position.

On average, we measured position distributions with a FWHM $=$ 1.8 mm and FWHM $=$ 1.9 mm for positions along the X- and Y-axis, respectively. A preliminary study concerning this topic can be found in a previous reference [25]. It is important to indicate that the results presented in this section correspond to the FWHM of the projection along the X and Y axes of the Point Spread Function. In this case we determine the interaction position event by event in the γ camera plane, obtaining one spot per collimated position after a set of events. The projection of this spot along the X and Y axes is the one shown in Fig. 11. We then calculate the FWHM and these are the results described in this section. This concept is different to the one presented in Table III, where we are talking about the light distribution width. As explained in Section V.A, in that case we accumulated the light distribution shapes of 10^6 events

and we normalized it afterwards. From this normalized light distribution we calculated the light distribution width from the Gaussian fit. This value is then fixed when the system works in a real situation, determining the interaction position event by event, such as for instance the situation presented here or in Fig. 7(c).

VI. Conclusion

In the current work, the study carried out on the performance of a γ camera made up of four PSDs with an individual anode readout proves that the light distribution has a Gaussian shape over the whole surface of the system with a constant width. The algorithm developed, based on the Gaussian fit to the experimental light distribution, provides sub-milimetric precision in the determination of the interaction position. In comparison to Anger's Logic, our algorithm enhances the field of view area, improving the quality of the image and maintaining a high performance even at the edges of the object to be scanned. We consider it to be shown as an alternative to Anger's Logic when a pixelated γ camera is used.

Acknowledgment

The authors would like to thank Dr. C. Domingo Pardo for his support during the development stage and D. Barrientos for his work at our laboratory at the beginning of SALSA.

References

[1] AGATA, "Advanced gamma tracking array," *Nucl. Intrum. Meth. Phys. Res. A,* vol. 668, pp. 26–58, 2012.
[2] Official GRETA homepage [Online]. Available: http://greta.lbl.gov
[3] M. Dimmock *et al.*, "Validation of pulse shape simulations for an AGATA prototype detector," *IEEE Trans. Nucl. Sci.*, vol. 56, no. 4, pp. 2415–2425, Aug. 2009.
[4] P. Suetens*, Fundamentals of Medical Imaging*. Cambridge, U.K.: Cambridge Univ. Press, 2009, ch. 5.
[5] C. Domingo-Pardo *et al.*, "A novel gamma-ray imaging method for the pulse-shape characterization of position sensitive semiconductor radiation detectors," *Nucl. Instrum. Meth. A*, vol. 643, pp. 79–88, 2011.
[6] H. O. Anger*, Rev. Sci. Instrum.*, vol. 29, pp. 27–33, 1958.
[7] N. J. Yasillo, R. N. Beck, and M. Cooper, "Design considerations for a single tube gamma camera," *IEEE Trans. Nucl. Sci.*, vol. 37, no. 2, pp. 609–615, Apr. 1990.
[8] G. Charpak and F. Sauli, "Multiwire proportional chambers and drift chambers," *Nucl. Instrum. Meth.*, vol. 162, pp. 405–428, 1979.
[9] R. A. Boie *et al.*, "High resolution X-ray gas proportional detectors with delay line position sensing for high counting rates," *Nucl. Instrum. Meth.*, vol. 201, pp. 93–115, 1982.
[10] B. Yu *et al.*, "Position sensitive gas proportional detectors with anode blades," *IEEE Trans. Nucl. Sci.*, vol. 46, no. 3, pp. 338–341, Jun. 1999.
[11] A. J. Bird, Z. He, and D. Ramsden, "Multi-channel readout of crossed-wire anode photomultipliers," *Nucl. Instrum. Meth. Phys. Res. A*, vol. 348, pp. 668–672, 1994.
[12] A. Truman and A. J. Bird *et al.*, "Pixellated CsI(Tl) arrays with position-sensitive PMT readout," *Nucl. Instrum. Meth. Phys. Res. A*, vol. 353, pp. 375–378, 1994.
[13] C. Domingo-Pardo *et al.*, "A position sensitive GAMMA-Ray scintillator detector with enhanced spatial resolution, linearity, and field of view," *IEEE Trans. Med. Imag.*, vol. 28, no. 12, pp. 2007–2014, Dec. 2009.
[14] R. Pani *et al.*, "Recent advances and future perspectives of position sensitive PMT," *Nucl. Instrum. Meth. Phys. Res. B*, vol. 213, pp. 197–205, 2004.
[15] R. J. Aliaga *et al.*, "Corrected position estimation in PET detector modules with multi-anode PMTs using neural networks," *IEEE Trans. Nucl. Sci.*, vol. 53, no. 3, pp. 776–783, Jun. 2006.
[16] R. Pani *et al.*, "High spatial and energy resolution gamma imaging based on LaBr3(Ce) continuous crystals," presented at the IEEE Nuclear Sci. Symposium Conference Record NM2-7, 2008.
[17] L. Pidol *et al.*, "High efficiency of lutetium silicate scintillators, Ce-doped LPS, and LYSO crystals," *IEEE Trans. Nucl. Sci.*, vol. 51, no. 3, pp. 1084–1087, Jun. 2006.
[18] Eckert and Ziegler, Co. Sources for Medical Imaging [Online]. Available: http://www.ezag.com/home/products/isotope-products
[19] R. Barth, Y. Du, H. Essel, R. Fitzsche, H. Gringer, J. Hoffmann, F. Humbert, N. Kurz, R. Mayer, W. Ott, and D. Schall, "GSI multi-branch system user manual," *GSI Helmholtzzentrum Schwerio-nenforschung GmbH*, Jan. 2000 [Online]. Available: http://www.win. gsi.de/daq/
[20] Creative Electronic Systems-CES [Online]. Available: http://www.ces.ch/
[21] J. Adamczewski, M. Al-Turany, D. Bertini, H. Essel, and S. Linev, "The Go4 analysis framework reference manual v4.0," *GSI Helmholtzzntrum Schwerionenforschung GmbH*, Feb. 2008 [Online]. Available: http://www-linux.gsi.de/go4
[22] R. Brun and F. Rademakers, "ROOT. An object oriented data analysis framework," *Nucl. Instrum. Meth. Phys. Res. A*, vol. 389, pp. 81–86, 1997.
[23] [Online]. Available: http://root.cern.ch/root/html/TMinuit.html
[24] W R. Hendee and E. Russell*, Medical Imaging Physics*, 4th ed. ed. Hoboken, NJ: Wiley, 2003.
[25] A. Hernandez-Prieto *et al.*, "Towards a deep characterization of a 64-fold-pixelated position sensitive detector for a new scanning system of HPGe segmented detectors," presented at the 2nd Int. Conf. Advancements in Nuclear Instrumentation Measurement Methods and their Applications (ANIMMA), 2011.